KFUPM
Journal of Undergraduate Research International

Diamond Open Access 123

Article Material Science and Engineering

Comprehensive Numerical Analysis of Highly Efficient Lead-Free $CH_3NH_3SnI_3$-Based Perovskite Solar Cell

Foyzul Karim[1], Md. Habibur Rahman Aslam[2] and Anisul Islam Suva[3]*

Cite https://doi.org/10.64589/juri/207995

Submitted: June 01, 2025 **Revised:** July 07, 2025 **Accepted:** August 19, 2025

ABSTRACT

Perovskite solar cells (PSCs) are highly efficient photovoltaic technologies, offering bandgap tunability and low production costs. However, lead toxicity, architectural limitations, and defect-induced recombination hinder their commercialization. This study investigates $CH_3NH_3SnI_3$ as a nontoxic absorber in an FTO/WSe_2/$CH_3NH_3SnI_3$/NiO/Au device architecture. Through systematic numerical simulations using Solar Cell Capacitance Simulator-1D (SCAPS-1D), the key design parameters—layer thicknesses, densities of doping, and defect concentrations—are carefully optimized. The resulting device structure exhibits a notable power conversion efficiency of 34.74%, V_{oc} of 1.1084 V, J_{sc} of 36.7788 mA/cm^2, fill factor of 85.22%, and peak quantum efficiency of 99.95% at 390 nm under AM 1.5G illumination. Sensitivity analysis reveals that both bulk ($N_t > 10^{14}$ cm^{-3}) and interface ($N_{int} > 10^{17}$ cm^{-3}) defects drastically degrade the performance, particularly at the $CH_3NH_3SnI_3$/WSe_2 interface. These findings have significant implications for highly efficient lead-free PSC designs.

Keywords: perovskite, photovoltaics, doping, defects, SCAPS-1D

1. INTRODUCTION

Solar energy has become the center of the world's search for green and sustainable energy substitutes in a bid to replace fossil fuels. Among cutting-edge photovoltaic (PV) technologies, perovskite solar cells (PSCs) have garnered considerable interest owing to their impressive power conversion efficiency (PCE), cost-effective fabrication, and amenability to scalable thin-film technologies [1,2]. Specifically, organic-inorganic halide PSCs have undergone dramatic efficiency improvements, rising from 3.8% to over 25% over the past decade, thus rivaling conventional silicon-based PV systems [3–5].

Despite these advances, the widespread adoption of PSCs is hindered by lead (Pb) toxicity in common absorbers, such as $CH_3NH_3PbI_3$, which poses major environmental and health risks [6–8]. This has stimulated research into nontoxic alternatives. The most promising lead-free alternative is $CH_3NH_3SnI_3$ (methylammonium tin iodide), a perovskite material with a 1.3 eV direct bandgap, excellent photon harvesting, and enhanced charge carrier mobility owing to its partially covalent Sn–I bond network [9–11]. These properties make $CH_3NH_3SnI_3$ a viable absorber for high-performance green PSCs.

However, $CH_3NH_3SnI_3$-based PSCs face several challenges. Sn^{2+} is easily oxidized to Sn^{4+}, reducing material stability and creating high-level defects that serve as recombination centers [12]. Additionally, bulk and interfacial defect densities continue to limit efficiency. Another key factor affecting device performance is the choice of charge transport layers (CTLs)—namely, the electron transport layer (ETL) and hole transport layer (HTL) [13]. Conventional ETLs (e.g., TiO_2) and HTLs (e.g., spiro-OMeTAD) suffer from low thermal stability, high financial cost, and degradation tendency under ambient conditions [13,14].

In this context, tungsten diselenide (WSe_2) has been presented as a high-performance ETL alternative. Owing to its favorable conduction band alignment, superior carrier mobility, good stability, and low defect density, WSe_2 can be used for electron transportation and extraction [15,16]. Coupled with thermostable NiO as the HTL, these inorganic CTL configurations contribute to enhanced performance in tin-based PSCs [17,18].

In this study, the Solar Cell Capacitance Simulator-1D (SCAPS-1D) was employed to optimize a lead-free FTO/WSe_2/$CH_3NH_3SnI_3$/NiO/Au structure. A detailed parametric study was conducted, examining the impacts of layer thickness, doping concentration, and density of defects on the PV performance metrics. Special emphasis was placed on quantifying and minimizing recombination losses, specifically at the absorber/ETL interface, to maximize the potential of lead-free PSCs.

2. METHODOLOGY

2.1. SCAPS-1D Simulation. Numerical analysis was performed with SCAPS-1D, a device modeling software created by the ELIS Department of Ghent University [19], to simulate and optimize tin-based PSC behavior. SCAPS-1D is renowned within

Published under an exclusive license by KFUPM

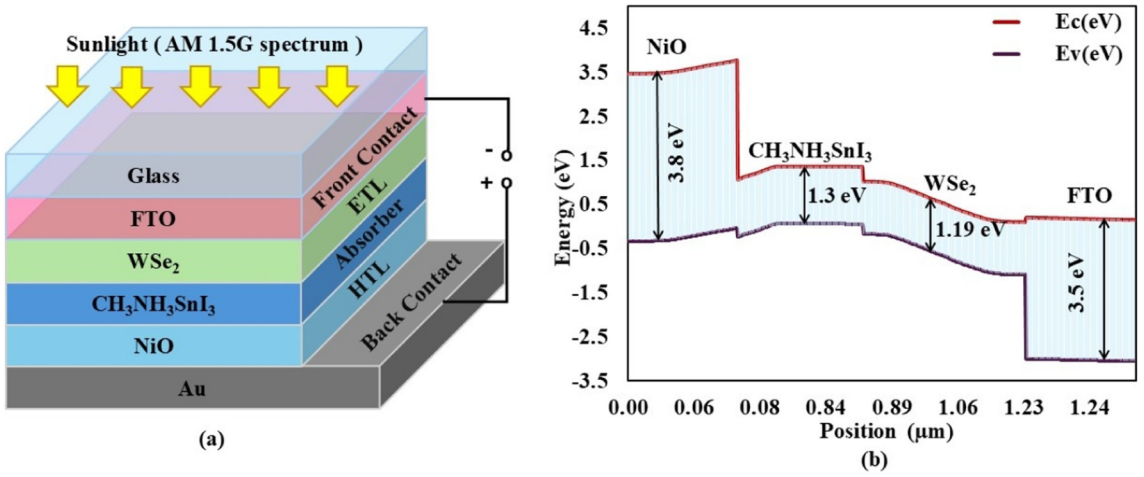

Figure 1. (a) Schematic representation and (b) energy band diagram of the designed PSC

the PV scientific community for its ability to simulate complex multilayer solar cell geometries by solving elementary semiconductor equations, that is, Poisson's equation (Eq. 1), hole continuity equation (Eq. 2), and electron continuity equation (Eq. 3), for steady-state conditions under AM 1.5G solar irradiation. Charge transport under an electric field and concentration gradients was simulated using the drift-diffusion equations (Eqs. 4 and 5). The simulator also encompasses key processes such as photon absorption, carrier generation, transport, recombination, and extraction at the interfaces. The incorporation of the Shockley–Read–Hall model enables the realistic treatment of defect-assisted recombination. These features enable the precise analysis of current–voltage (J–V) characteristics, quantum efficiency (QE), and recombination dynamics.

$$\frac{d^2\Psi(x)}{dx^2} = \frac{q}{\epsilon_o \epsilon_r}[p(x) - n(x) + N_D - N_A + \rho_p - \rho_n] \quad (1)$$

$$\frac{\delta p}{\delta t} = \frac{1}{q}\frac{\delta J_p}{\delta x} + G_p - R_p \quad (2)$$

$$\frac{\delta n}{\delta t} = \frac{1}{q}\frac{\delta J_n}{\delta x} + G_n - R_n \quad (3)$$

$$J_n(x) = q\mu_n n(x)\varepsilon(x) + qD_n\frac{dn(x)}{dx} \quad (4)$$

$$J_p(x) = q\mu_p p(x)\varepsilon(x) + qD_p\frac{dp(x)}{dx} \quad (5)$$

where

Ψ denotes the electrostatic potential

q represents the elementary charge

ε_o and ε_r are the vacuum permittivity and the material's relative permittivity, respectively

p and n indicate hole and electron concentrations

N_D and N_A are the donor and acceptor doping concentrations

ρ_p and ρ_n signify hole and electron charge concentrations

J_p and J_n refer to the current densities

G_p and G_n are the respective generation rates

R_p and R_n correspond to the recombination rates

μ_n and μ_p are the mobilities of electrons and holes

$\varepsilon(x)$ describes the electric field as a function of position

D_n and D_p are the diffusion coefficients

2.2. Basic Structure, Operation, and Input Parameters. Figure 1(a) shows the multilayer configuration of $CH_3NH_3SnI_3$-based PSC. The device comprises fluorine-doped tin oxide (FTO) as the front electrode, WSe_2 as the ETL, $CH_3NH_3SnI_3$ as the lead-free light-absorbing perovskite, NiO as the HTL, and gold (Au) as the back contact. Upon illumination, the perovskite layer generates electron–hole pairs by absorbing the incoming photons. Electrons are channeled through ETL to the FTO electrode, while holes are transferred via HTL to the Au contact owing to the photovoltaic effect. Carrier recombination, particularly at interfaces, may cause degradation; thus, optimization of the layer thickness, materials, and interface quality is required. The energy band diagram (Figure 1(b)) demonstrates well-aligned energy levels among the device layers. Conduction band alignment of WSe_2 and $CH_3NH_3SnI_3$ facilitates efficient electron extraction, whereas NiO enables efficient hole extraction and electron blocking, enhancing selectivity and reducing recombination losses.

The rear gold contact, with a work function of 5.10 eV, was suitably positioned to facilitate hole collection from the HTL. The material-dependent input parameters for all the layers, that is, FTO, ETL, absorber, HTL, and interface defects, which constitute the reference dataset, are listed in Tables 1 and 2.

3. RESULTS AND DISCUSSION

3.1. Effect of Layer Thickness on Photovoltaic Efficiency. The thickness of individual layers is highly sensitive to the performance of $CH_3NH_3SnI_3$-based PSCs. To assess their impact, SCAPS-1D simulations were conducted by adjusting one layer at a time while keeping the others fixed. Key performance indicators—open-circuit voltage (V_{oc}), short-circuit current (J_{sc}), fill factor (FF), and PCE—were investigated (Figures 2 and 3).

3.1.1. Influence of Absorber and HTL Thickness. The absorber thickness was elevated from 0.6 to 1.0 µm, keeping the remaining layers fixed at 0.05 µm. As shown in Figure 2(a), V_{oc} declines from 1.0370 to 1.0248 V because of the increased recombination in thick films. J_{sc} marginally improves (Figure 2(b)), with the maximum at 34.981 mA/cm^2 at 1.0 µm,

Table 1. *Material properties for FTO, ETL, absorber, HTL*

Material property	FTO[20]	WSe_2[21]	$CH_3NH_3SnI_3$[22]	NiO[23]
Thickness [nm]	50	150	1000	100
Bandgap, E_g [eV]	3.5	1.19	1.3	3.8
Electron affinity, X [eV]	4.40	4.50	4.17	1.46
Relative dielectric permittivity, ϵ_r	9.00	13.80	8.20	11.7
Effective density of states for conduction band N_C (cm^{-3})	2.2×10^{18}	8.3×10^{18}	1×10^{18}	2.5×10^{20}
Effective density of states for Valence band N_V (cm^{-3})	1.8×10^{19}	1.6×10^{16}	1×10^{18}	2.5×10^{20}
Thermal velocity of electron (cms^{-1})	10^7	10^7	10^7	10^7
Thermal velocity of hole (cms^{-1})	10^7	10^7	10^7	10^7
Mobility of electron, μ_n ($cm^2\ Vs^{-1}$)	20	100	1.6	2.8
Mobility of hole, μ_h ($cm^2\ Vs^{-1}$)	10	500	1.6	2.8
Donor concentration, N_D ($1\ cm^{-3}$)	10^{16}	10^{18}	-	-
Acceptor concentration, N_A ($1\ cm^{-3}$)	-	-	10^{16}	10^{16}
Density of the defect, N_t (cm^{-3})	10^{15}	10^{15}	10^{14}	10^{15}

Table 2. *Parameters for interface defect layers*

Interface	$NiO/CH_3NH_3SnI_3$	$CH_3NH_3SnI_3/WSe_2$
Defect type	Neutral	Neutral
Capture Cross Section: Electrons/holes [cm^2]	1.0×10^{-19}	1.0×10^{-19}
Energetic distribution	Single	Single
Reference for defect energy level	Above the VB maximum	Above the VB maximum
Energy level relative to reference (eV)	0.6	0.6
Total density [cm^{-2}] (integrated over all energies)	1.0×10^{10}	1.0×10^{10}

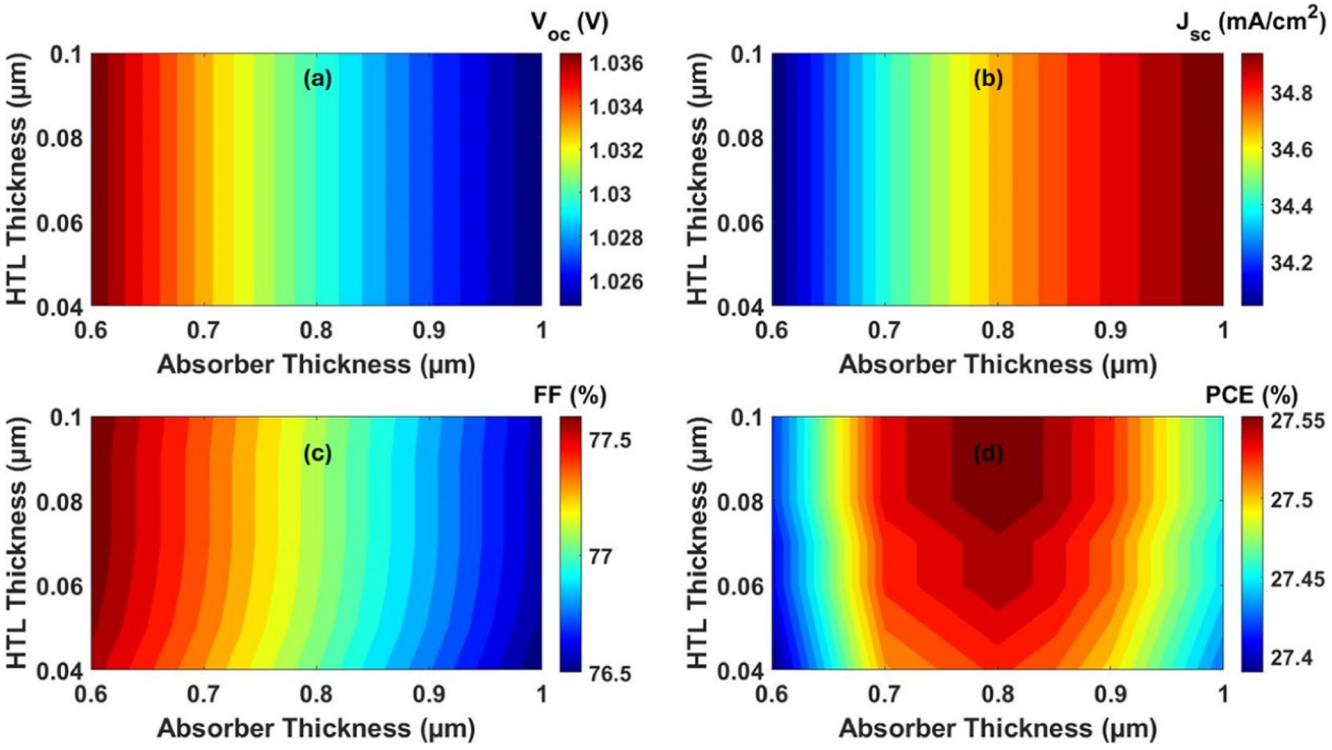

Figure 2. Relation of absorber and HTL thickness on PV performance

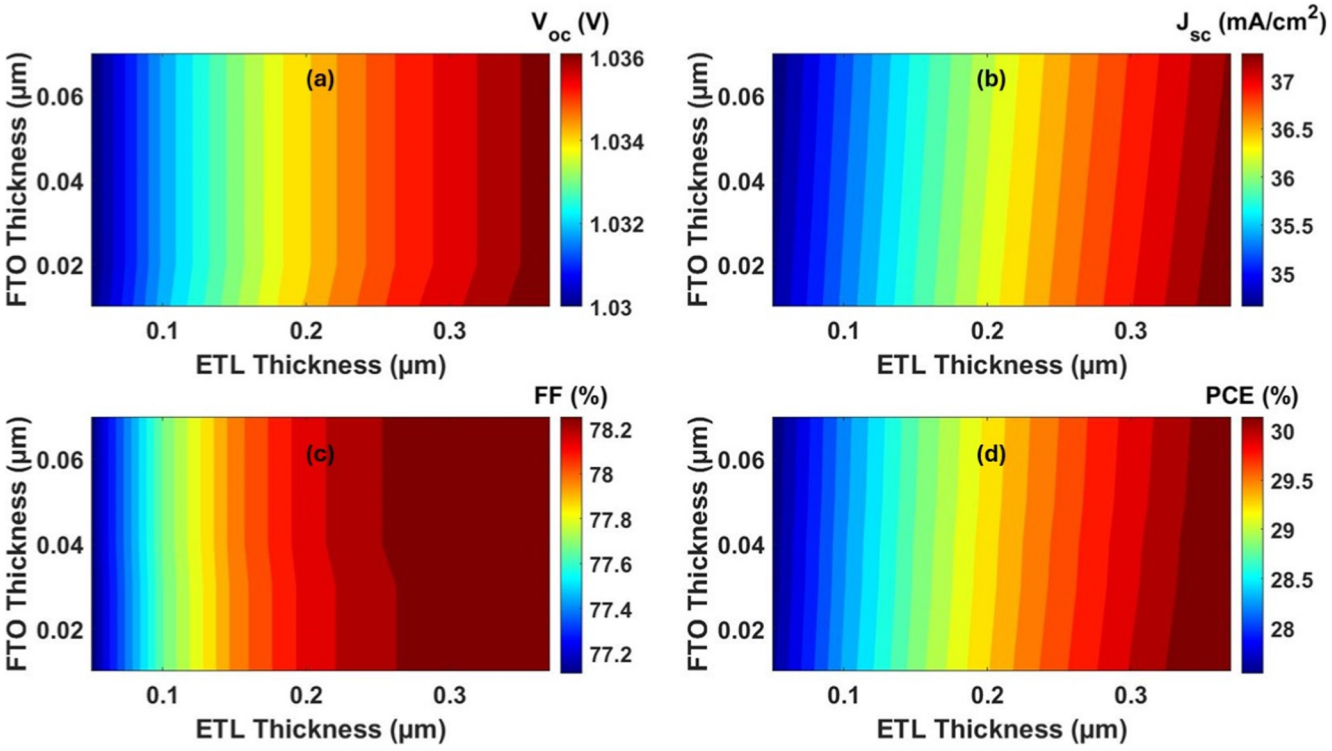

Figure 3. Relation of ETL and FTO thickness on PV performance

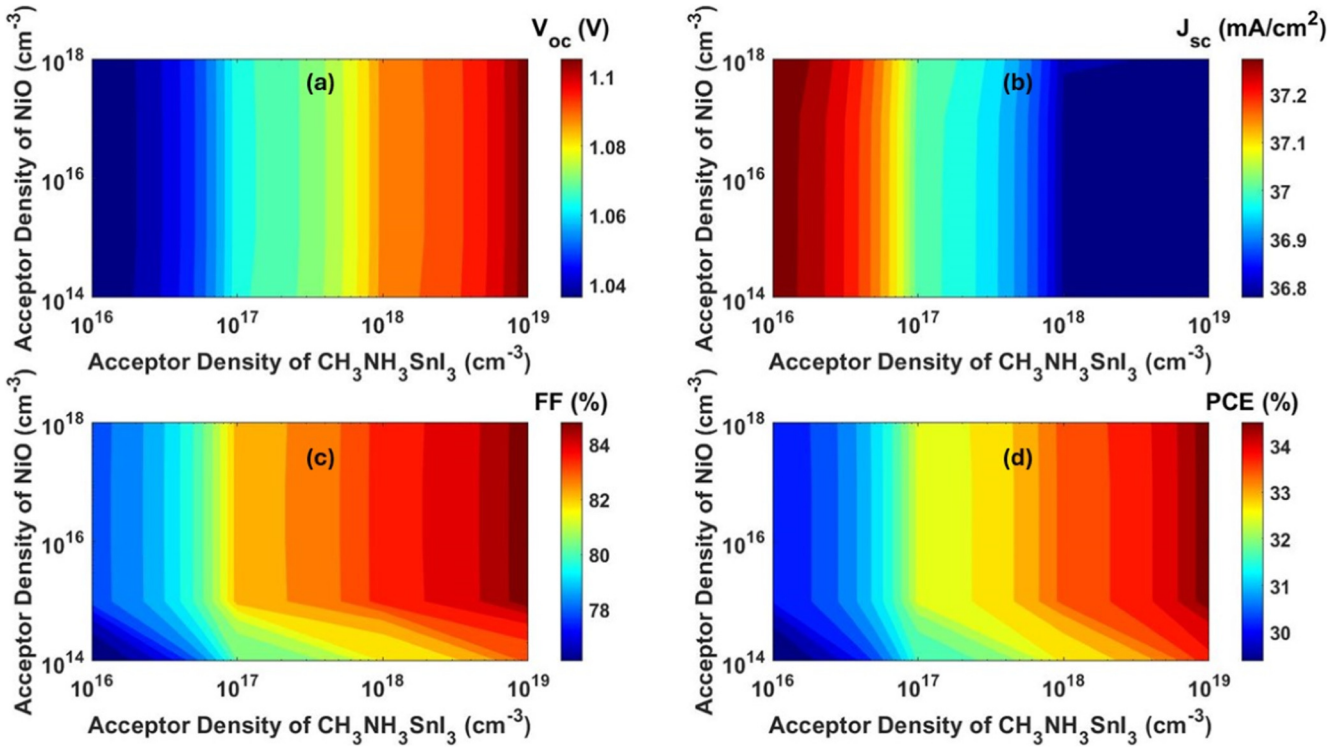

Figure 4. Relation of acceptor density of absorber and HTL on PV performance

but the improvement tails off beyond 0.8 μm. The FF decreases from 77.61% to 76.54% (Figure 2(c)) because of the series resistance effects. Accordingly, PCE achieves a top of 27.54% at 0.8 μm, which is the best balance between V_{oc}, J_{sc}, and FF (Figure 2(d)).

By immobilizing the absorber at 0.8 μm, changing the thickness of HTL from 0.04 to 0.10 μm produced small impacts on V_{oc} and J_{sc} (Figure 2(a) and 2(b)), both of which remained at constant values of ~1.030 V and 34.688 mA/cm^2. However, FF was slightly increased with a peak value of 77.13% at 0.10 μm

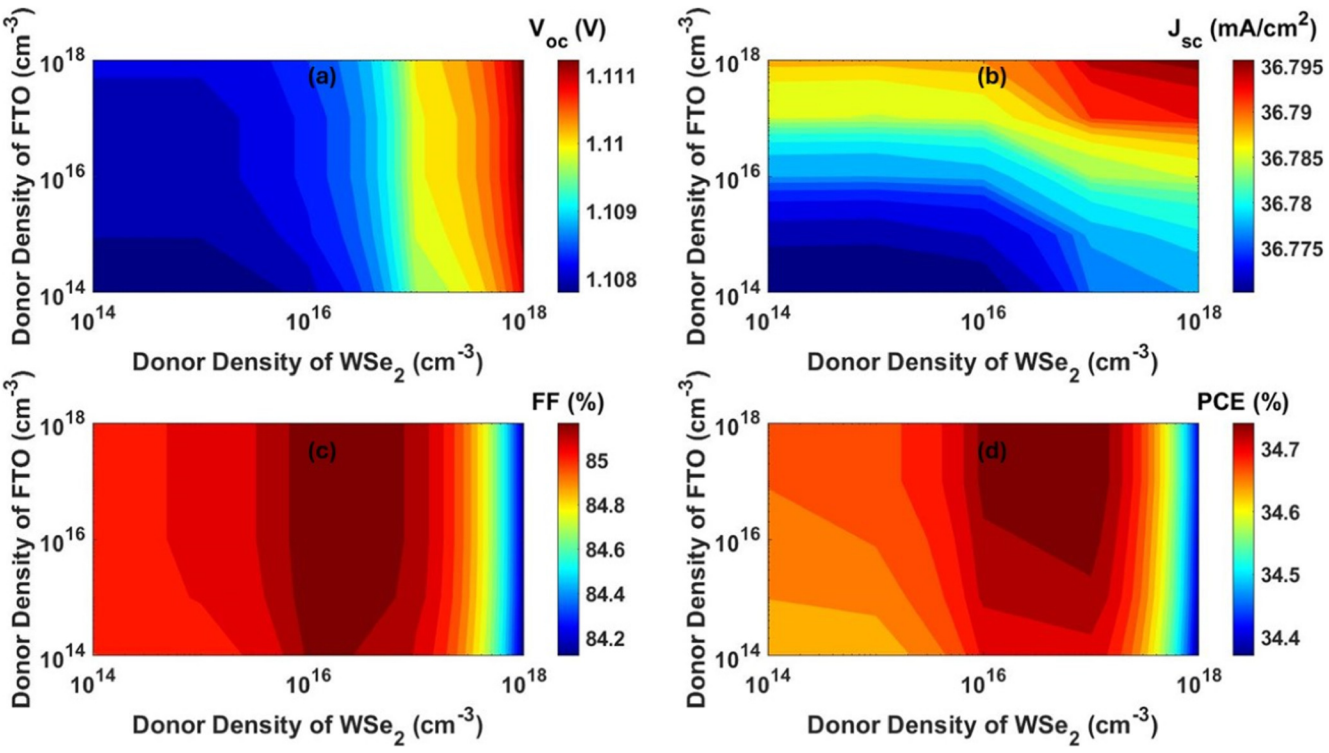

Figure 5. Relation of donor density of ETL and FTO on PV performance

(Figure 2(c)), leading to a highest PCE of 27.56% at 0.08 µm (Figure 2(d)).

3.1.2. Influence of ETL and FTO Thickness. The absorber and HTL were set at their optimal values, and the ETL thickness varied between 0.05 and 0.37 µm. V_{oc} rose from 1.0300 to 1.0361 V (Figure 3(a)), J_{sc} increased to 37.228 mA/cm^2 (Figure 3(b)), and FF increased to 78.31% (Figure 3(c)). The best PCE (30.20%) was achieved with a 0.35 µm ETL thickness (Figure 3(d)).

After optimizing all other layers, FTO thickness reduction to 0.01 µm improved J_{sc} to 37.305 mA/cm^2 (Figure 3(b)) owing to improved light transmission. V_{oc} and FF remained unchanged, resulting in a maximum PCE of 30.27% at 0.01 µm FTO (Figure 3(d)).

3.1.3. Optimized Layer Thickness Design. Simulation data reveal the optimal configuration: absorber thickness 0.8 µm, HTL (NiO) 0.08 µm, ETL (WSe_2) 0.35 µm, and FTO 0.01 µm, yielding V_{oc} = 1.0362 V, J_{sc} = 37.3054 mA/cm^2, FF = 78.30%, and PCE = 30.27%.

3.2. Impact of Doping Concentrations. The doping density is a crucial factor influencing the internal electric field, carrier behavior, and efficiency of PSCs. We investigated the impact of various doping densities on each functional layer of the designed PSC. The contour plots in Figures 4 and 5 show the key PV parameters, such as V_{oc}, J_{sc}, FF, and PCE.

3.2.1. Impact of Absorber and HTL Acceptor Doping Density. As shown in Figure 4, an increase in the absorber's acceptor doping concentration from 10^{16} to 10^{19} cm^{-3} enhances V_{oc} substantially by increasing it from 1.0362 V to 1.1084 V. This trend is attributed to the reduced nonradiative recombination and enhanced built-in potential. The J_{sc} remains relatively unchanged (37.288–36.779 mA/cm^2), indicating that charge generation and light absorption remained efficient. The FF also increases dramatically from 78.12% to 85.23%, and the total PCE increases from 30.18% to 34.74%. The optimum absorber doping concentration is therefore 10^{19} cm^{-3}.

Figure 4 also shows the impact of varying NiO doping concentrations on key performance parameters. V_{oc} and J_{sc} are considerably stable in the range 10^{14}–10^{18} cm^{-3}, but FF increases with greater doping and reaches a value of 85.23%. PCE saturates for greater doping values above 10^{15} cm^{-3}; thus, 10^{15} cm^{-3} is set as the optimum HTL doping concentration.

3.2.2. Impact of Donor Doping Density of ETL and FTO. Figure 5 shows the donor doping effect on the ETL. An increase in the density of donors from 10^{14} to 10^{16} cm^{-3} enhances V_{oc} and FF, resulting in a PCE of 34.74%. With further increased concentration of doping, e.g., 10^{17}–10^{18} cm^{-3}, FF decreases slightly despite minor increases in V_{oc} owing to increased recombination or carrier transport imbalance. Therefore, 10^{16} cm^{-3} is determined as the optimal concentration for doping.

Figure 5 further shows the performance trend with FTO doping levels (10^{14}–10^{18} cm^{-3}). V_{oc}, J_{sc}, and FF exhibited little variation. The change is minimal (< 0.04%), and the values stabilized at 34.74%. Thus, the FTO conductivity is not a limiting factor within the range considered here, and 10^{16} cm^{-3} is satisfactory for efficient performance.

3.2.3. Optimized Doping Configuration. The simulated result proposes the following optimum levels of doping for each layer: absorber at 10^{19} cm^{-3}, HTL at 10^{15} cm^{-3}, ETL at 10^{16} cm^{-3}, and FTO at 10^{16} cm^{-3}. Using this configuration, an

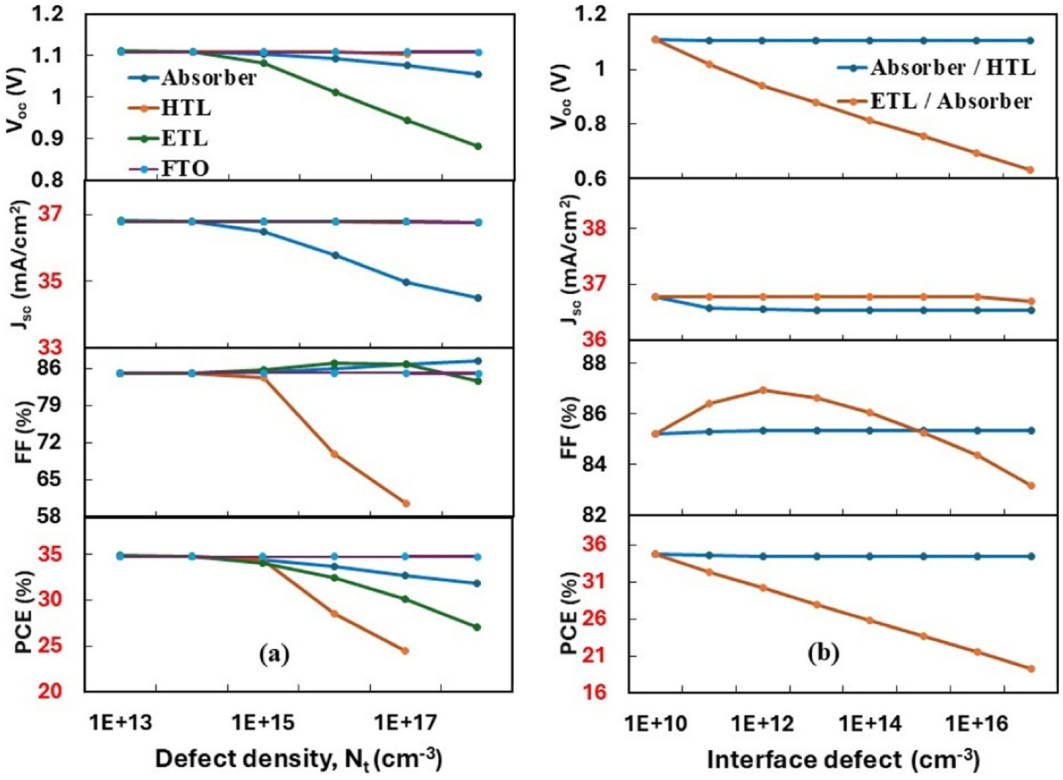

Figure 6. Effect of (a) bulk defect density (N_t) and (b) interface defect density (N_{int}) on PV performance

optimal PCE of 34.74% is achieved, demonstrating the significance of controlled doping in high-efficiency lead-free PSCs.

3.3. Effects of Defect Densities on Photovoltaic Performance. The efficiency and operational stability of $CH_3NH_3SnI_3$-based PSCs are markedly influenced by defect density within both the bulk absorber layer and its interfacial regions. The bulk (N_t) and interface (N_{int}) defect densities act as nonradiative recombination centers and affect the PV performance, as shown in Figure 6.

3.3.1. Defect Density (N_t) Effects. The absorber is highly sensitive to N_t variation between 10^{13} and 10^{18} cm^{-3}. As N_t increases, V_{oc} declines from 1.1089 V to 1.0564 V (−4.74%), and J_{sc} decreases from 36.820 to 34.508 mA/cm^2 (−6.28%). This performance degradation is primarily attributed to elevated trap-assisted recombination, which reduces the quasi-Fermi level splitting. The performance is relatively stable up to $N_t = 10^{14}$ cm^{-3}, although there is degradation that begins dominantly at $N_t \geq 10^{15}$ cm^{-3}. J_{sc} and N_t have a strong negative correlation,

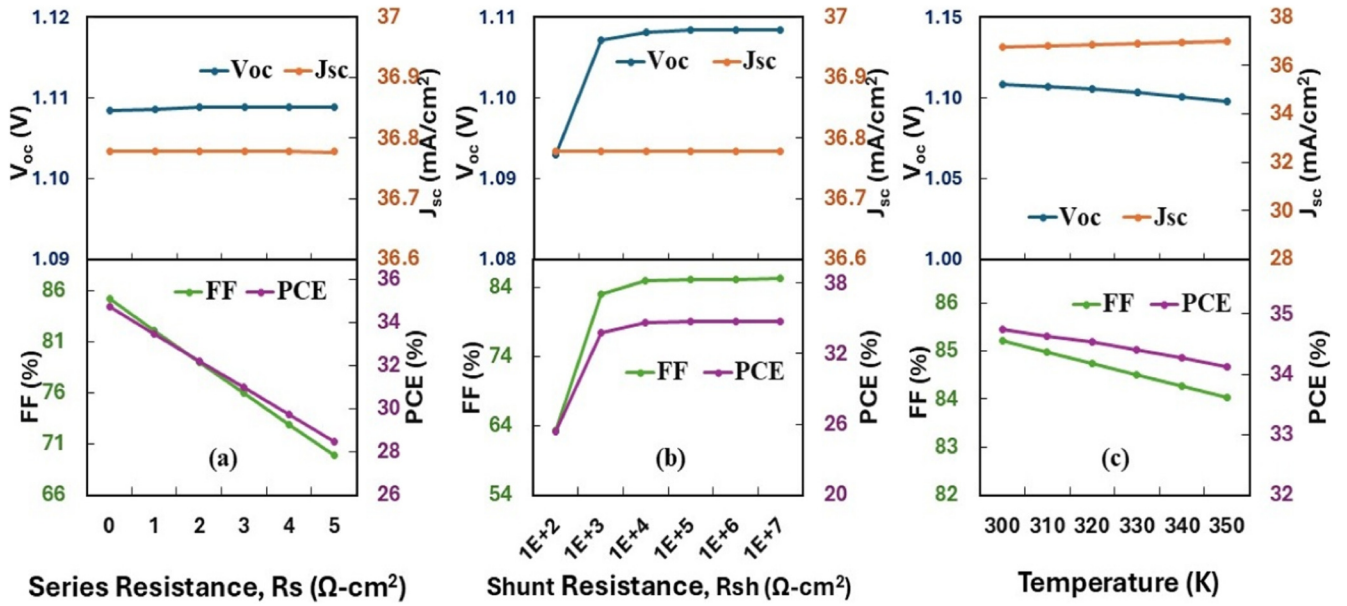

Figure 7. Impact of (a) series resistance (Rs), (b) shunt resistance (Rsh), and (c) temperature on PV performance

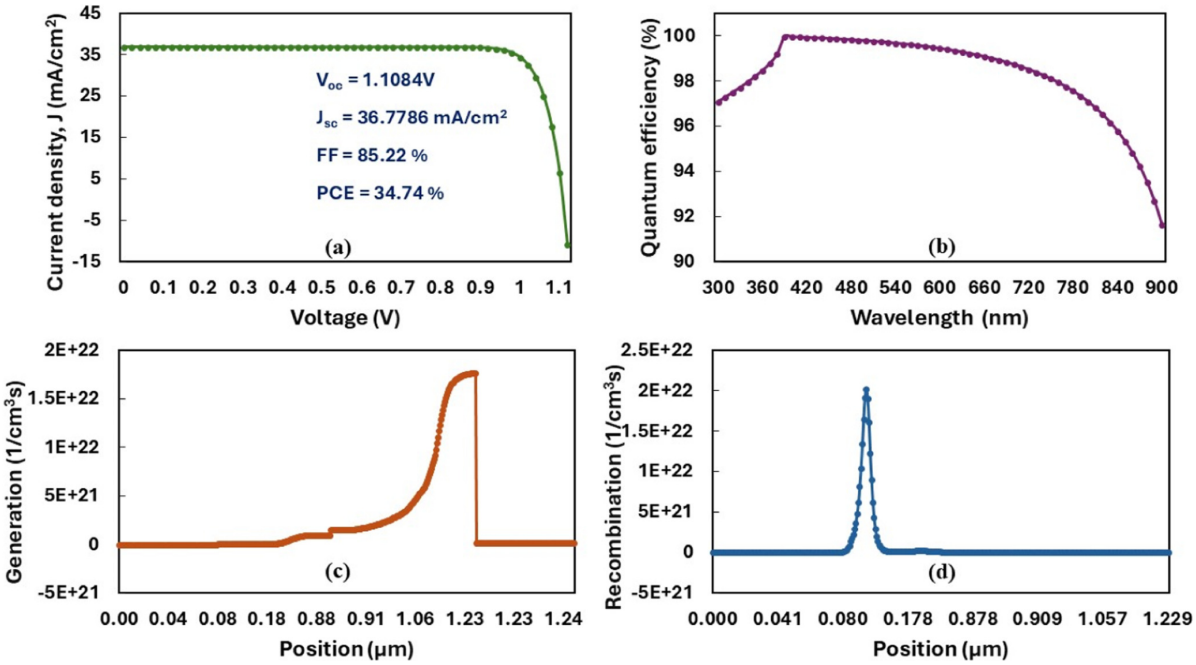

Figure 8. (a) J–V characteristics curve, (b) quantum efficiency curve, (c) generation curve, and (d) recombination curve for the optimized PSC model

Table 3. *Performance comparison of optimized PSC with existing literature*

Structure	V_{OC} (Volt)	J_{sc} (mA/cm^2)	FF (%)	PCE (%)	Ref.
ITO/ ZnO/ CdTe/ $CH_3NH_3SnI_3$/ CuSCN/ Au	0.8150	34.050	76.57	21.24	24
FTO/ NiO/ $CH_3NH_3SnI_3$/ PCBM/ Al	0.9760	33.450	70.33	22.95	25
TCO/ TiO_2/ $CH_3NH_3SnI_3$/ Spiro-OMeTAD/ BC	0.920	31.590	79.99	23.36	26
FTO/ TiO_2/ $CH_3NH_3SnI_3$/ Spiro-OMeTAD/ BC	0.890	35.320	77.45	24.36	27
FTO/ CdS/ $CH_3NH_3SnI_3$/ Cu_2O/ Pt	0.8780	33.40	85.25	25.02	28
TCO/ TiO_2/ $CH_3NH_3SnI_3$/ CuO/ Au	0.930	34.420	83.61	26.63	29
TiO_2/ $CH_3NH_3SnI_3$/ Cu_2O/ Pt	1.020	32.60	84.05	27.95	30
FTO/ TiO_2/ $CH_3NH_3SnI_3$/ Cu_2O/ Pt	0.930	40.14	75.78	28.39	31
FTO/ WSe_2/ $CH_3NH_3SnI_3$/ NiO/ Au	1.1084	36.7788	85.22	34.74	PW

**Note: PW = Present Work*

which indicates carrier collection losses owing to bulk recombination. Devices are supported with < 1% PCE loss if N_t is kept below 10^{15} cm^{-3}.

The HTL shows low sensitivity to N_t values up to 10^{15} cm^{-3}, with V_{oc} and J_{sc} remaining nearly invariant. However, for values greater than this, the FF falls precipitously from 84.35% to 69.96%, with PCE falling from 34.74% to 28.52%. The results show that for V_{oc} and J_{sc} under stable conditions, defect-induced recombination reduces the efficiency of charge transport.

ETL demonstrates significant V_{oc} degradation from 1.1124 V to 0.8815 V (−20.76%) at $N_t = 10^{18}$ cm^{-3}, while J_{sc} is not significantly affected. This implies that defects degrade voltage generation without significantly affecting photon absorption or carrier generation. Optimal N_t must be below 10^{14} cm^{-3} for ETL. The FTO contact was highly stable, with negligible variation in all performance parameters across six orders of magnitude in N_t.

3.3.2. Interface Defect Density (N_{int}) Effects. The NiO/$CH_3NH_3SnI_3$ interface is highly N_{int} resistant up to 10^{17} cm^{-3}, with a PCE loss of less than 0.7%, and V_{oc} and J_{sc} remaining below 2%. Contrastingly, the $CH_3NH_3SnI_3$/WSe_2 interface is sensitive; V_{oc} decreases from 1.1084 V to 0.6351 V (−42.7%) as N_{int} increases from 10^{10} to 10^{17} cm^{-3}, with a PCE loss of 44.2%. This highlights the immediate need for interface defect passivation on the ETL side.

3.4. Influence of Series Resistance, Shunt Resistance, and Temperature on PV Parameters. Figure 7 shows the parasitic resistances and temperature sensitivities of important PV parameters. As shown in Figure 7(a), increasing the series resistance (Rs) induces a sharp drop in both FF and PCE, whereas V_{oc} and J_{sc} are relatively stable. In contrast, a higher shunt resistance (Rsh) significantly enhances the performance by curbing leakage losses, as shown in Figure 7(b). Figure 7(c) indicates that temperature variation optimizes performance under moderate-level conditions and deteriorates under elevated temperatures because of increased recombination.

3.5. Enhanced PV Parameters and Carrier Dynamics Analysis of Optimized PSC. The optimized PSC was investigated in depth using the J–V characteristics, QE, carrier generation, and recombination profiles (Figure 8). The J–V curve (Figure 8(a)) under AM 1.5G illumination demonstrates high device performance, achieving a V_{oc} of 1.1084 V, J_{sc} of 36.7788 mA/cm^2, FF of 85.22%, and PCE of 34.74%, owing to effective charge extraction and good band alignment. The QE spectrum (Figure 8(b)) peaks at 99.95% at a wavelength of 390 nm and gradually decreases to 91.63% at 900 nm, exhibiting strong absorption across the visible range. Carrier generation is confined to the absorber layer (Figure 8(c)), and the minimum generation occurs in the transport layers. Figure 8(d) shows a distinct recombination peak at the absorber near the HTL/absorber interface, suggesting the requirement of passivating defects to maximize efficiency.

The current FTO/WSe_2/$CH_3NH_3SnI_3$/NiO/Au structure performs better than most previously reported $CH_3NH_3SnI_3$-based PSCs because of its extremely high PCE under AM 1.5G illumination (Table 3).

4. CONCLUSIONS

This study presents an in-depth numerical optimization of lead-free $CH_3NH_3SnI_3$-based PSC using SCAPS-1D simulations, focusing on structural, electrical, and defect-related parameters. The optimized structure shows an impressive PCE of 34.74% under AM 1.5G illumination conditions, with a V_{oc} of 1.1084 V, J_{sc} of 36.7788 mA/cm^2, FF of 85.22%, and peak quantum efficiency of 99.95% at 390 nm, surpassing the previously reported values of $CH_3NH_3SnI_3$-based PSCs.

The optimized parameters are as follows: the thickness of the absorber is 0.8 μm, NiO is 0.08 μm, WSe_2 is 0.35 μm, and FTO is 0.01 μm, with corresponding doping concentrations of 10^{19} cm^{-3} (absorber), 10^{15} cm^{-3} (HTL), 10^{16} cm^{-3} (ETL), and 10^{16} cm^{-3} (FTO). These conditions enhance carrier mobility, minimize nonradiative recombination, and promote efficient charge extraction.

Defect analysis showed the necessity of defect passivation because bulk defect densities above 10^{14} cm^{-3} at the absorber and interface defect densities above 10^{17} cm^{-3}—particularly at the $CH_3NH_3SnI_3$/WSe_2 interface—led to a 44.2% loss in PCE. In contrast, the HTL and FTO layers were defect-tolerant, demonstrating their robustness in device operation.

These findings provide a promising design framework for high-efficiency, environmentally benign, and lead-free PSCs, emphasizing the importance of optimized geometries, doping profiles, and defect control in advancing practical perovskite photovoltaic technologies.

AFFILIATIONS AND AUTHOR DETAILS

Undergraduate Author

Foyzul Karim – *Electrical and Electronic Engineering, Chittagong University of Engineering & Technology (CUET), 4349, Chittagong, Bangladesh;* 0009-0007-8318-0519
Email: u1902169@student.cuet.ac.bd

Md. Habibur Rahman Aslam – *Electrical and Electronic Engineering, Chittagong University of Engineering & Technology (CUET), Bangladesh;* 0009-0008-0751-9645
Email: u1902135@student.cuet.ac.bd

Corresponding Author

Anisul Islam Suva – *Research Mentor, Research Assistant Professor, Institute of Energy Technology, Chittagong University of Engineering & Technology (CUET), Bangladesh;* 0009-0000-7967-7548
Email: anisulislam.me@cuet.ac.bd

ACKNOWLEDGEMENTS

The authors acknowledge the use of the SCAPS-1D simulation software in this study and sincerely thank Dr. Marc Burgelman of Ghent University, Belgium, for his generous provision of access to this valuable tool for the broader scientific community.

CONFLICTS OF INTEREST AND FINANCIAL DISCLOSURE

The authors declare no conflict of interest. This study was conducted independently and did not receive any external funding.

REFERENCES

(1) Olabi, A. G., et al. "Renewable energy systems: Comparisons, challenges and barriers, sustainability indicators, and the contribution to UN sustainable development goals." *International Journal of Thermofluids* 20 (2023): 100498.

(2) Hu, Zhelu, et al. "The current status and development trend of perovskite solar cells." *Engineering* 21 (2023): 15–19.

(3) Kojima, Akihiro, et al. "Organometal halide perovskites as visible-light sensitizers for photovoltaic cells." Journal of the american chemical society 131.17 (2009): 6050–6051.

(4) Kim, Gi-Hwan, and Dong Suk Kim. "Development of perovskite solar cells with >25% conversion efficiency." *Joule* 5.5 (2021): 1033–1035.

(5) Machín, Abniel, and Francisco Márquez. "Advancements in photovoltaic cell materials: silicon, organic, and perovskite solar cells." *Materials* 17.5 (2024): 1165.

(6) Mandadapu, Usha, et al. "Design and simulation of high efficiency tin halide perovskite solar cell." *Int. J. Renew. Energy Res* 7.4 (2017): 1603–1612.

(7) Hima, Abdelkader, and Nacereddine Lakhdar. "Enhancement of efficiency and stability of CH3NH3GeI3 solar cells with CuSbS2." *Optical Materials* 99 (2020): 109607.

(8) Dutta, Sriman, and Saurabh Kumar Pandey. "Device Engineering and Materials Perspective Analysis of Highly Efficient Lead-Free $MASnI_3$ Perovskite Solar Cell." *IEEE Journal of Selected Topics in Quantum Electronics* 30.3: Flexible Optoelectronics (2023): 1–6.

(9) Jayan, K. Deepthi, and Varkey Sebastian. "Comprehensive device modelling and performance analysis of $MASnI_3$ based perovskite solar cells with diverse ETM, HTM and back metal contacts." *Solar Energy* 217 (2021): 40–48.

(10) Ke, Weijun, and Mercouri G. Kanatzidis. "Prospects for low-toxicity lead-free perovskite solar cells." *Nature communications* 10.1 (2019): 965.

(11) Alipour, Hossein, and Abbas Ghadimi. "Optimization of lead-free perovskite solar cells in normal-structure with WO_3 and water-free PEDOT: PSS composite for hole transport layer by SCAPS-1D simulation." *Optical Materials* 120 (2021): 111432.

(12) Mahmoudi, Tahmineh, et al. "Suppression of Sn_{2+}/Sn_{4+} oxidation in tin-based perovskite solar cells with graphene-tin quantum dots composites in active layer." *Nano Energy* 90 (2021): 106495.

(13) Hossain, M. Khalid, et al. "An extensive study on multiple ETL and HTL layers to design and simulation of high-performance lead-free $CsSnCl_3$-based perovskite solar cells." *Scientific Reports* 13.1 (2023): 2521.

(14) Fatima, Qawareer, et al. "A critical review on advancement and challenges in using TiO_2 as electron transport layer for perovskite solar cell." *Materials Today Sustainability* (2024): 100857.

(15) Paul, Indrojit, Abu Rayhan, and M. A. Khan. "Design and Performance Analysis of Photovoltaic Solar Cells Using WSe_2 as an Absorber Layer with SnS_2 Electron Transport Layer." *New Energy Exploitation and Application* 4.1 (2025): 83–101.

(16) Morshed, Md Saklain, Kanak Kanti Bhowmik, and Md Shafiqul Islam. "Investigation of MoS_2/Perovskite/WSe_2 on Si Tandem Structure of Solar Cell." *2022 12th International Conference on Electrical and Computer Engineering (ICECE)*. IEEE, 2022.

(17) Danjumma, Sani Garba, Yakubu Abubakar, and Sahabi Suleiman. "Nickel oxide (NiO) devices and applications: a review." *J. Eng. Res. Technol* 8 (2019): 12–21.

(18) Mitoff, S. P. "Electrical conductivity and thermodynamic equilibrium in nickel oxide." The Journal of Chemical Physics 35.3 (1961): 882-889.

(19) Niemegeers, A.; Burgelman, M.; Decock, K.; Verschraegen, J.; Degrave, S. SCAPS Manual. Ph.D. Thesis, University of Gent, Gent, Belgium, 2014. https://scaps.elis.ugent.be/

(20) Alam, Intekhab, Rahat Mollick, and Md Ali Ashraf. "Numerical simulation of $Cs_2AgBiBr_6$-based perovskite solar cell with ZnO nanorod and P3HT as the charge transport layers." *Physica B: Condensed Matter* 618 (2021): 413187.

(21) Gautam, Sakshi, et al. "Performance analysis of WSe_2 solar cell with Cu_2O hole transport layer by optimization of electrical and optical properties." *Journal of Computational Electronics* 21.6 (2022): 1373–1385.

(22) Mehrabian, Masood, Elham Norouzi Afshar, and Omid Akhavan. "TiO_2 and C_{60} transport nanolayers in optimized Pb-free $CH_3NH_3SnI_3$-based perovskite solar cells." *Materials Science and Engineering: B* 287 (2023): 116146.

(23) Ahmmed, Shamim, et al. "Enhancing the open circuit voltage of the SnS based heterojunction solar cell using NiO HTL." *Solar Energy* 207 (2020): 693–702.

(24) Qasim, Irfan, et al. "Design and numerical investigations of eco-friendly, non-toxic (Au/CuSCN/$CH_3NH_3SnI_3$/CdTe/ZnO/ITO) perovskite solar cell and module." *Solar Energy* 237 (2022): 52–61.

(25) Shamna, M. S., K. S. Nithya, and K. S. Sudheer. "Simulation and optimization of $CH_3NH_3SnI_3$ based inverted perovskite solar cell with NiO as Hole transport material." *Materials Today: Proceedings* 33 (2020): 1246–1251.

(26) Du, Hui-Jing, Wei-Chao Wang, and Jian-Zhuo Zhu. "Device simulation of lead-free $CH_3NH_3SnI_3$ perovskite solar cells with high efficiency." *Chinese Physics B* 25.10 (2016): 108802.

(27) Sahoo, Arpita, Ipsita Mohanty, and Sutanu Mangal. "Effect of acceptor density, thickness and temperature on device performance for tin-based perovskite solar cell." *Materials Today: Proceedings* 62 (2022): 6210–6215.

(28) Arif, Fozia, et al. "Simulation and numerical modeling of high performance $CH_3NH_3SnI_3$ solar cell with cadmium sulfide as electron transport layer by SCAPS-1D." *Results in Optics* 14 (2024): 100595.

(29) Imani, Shayesteh, et al. "Simulation and characterization of $CH_3NH_3SnI_3$-based perovskite solar cells with different Cu-based hole transporting layers." *Applied Physics A* 129.2 (2023): 143.

(30) Omarova, Zhansaya, et al. "In silico investigation of the impact of hole-transport layers on the performance of $CH_3NH_3SnI_3$ perovskite photovoltaic cells." *Crystals* 12.5 (2022): 699.

(31) Patel, Piyush K. "Device simulation of highly efficient eco-friendly $CH_3NH_3SnI_3$ perovskite solar cell." *Scientific reports* 11.1 (2021): 3082.